European Heart Journal – Cardiovascular Imaging (2013) **14**, 986–995
doi:10.1093/ehjci/jet004

Three-dimensional dynamic assessment of tricuspid and mitral annuli using cardiovascular magnetic resonance

Francesco Maffessanti[1]*, Paola Gripari[1], Gianluca Pontone[1], Daniele Andreini[1], Erika Bertella[1], Saima Mushtaq[1], Gloria Tamborini[1], Laura Fusini[1], Mauro Pepi[1], and Enrico G. Caiani[2]

[1]Centro Cardiologico Monzino IRCCS, Via Parea 4, Milan 20138, Italy; and [2]Department of Biomedical Engineering, Politecnico di Milano, Milan, Italy

Received 10 October 2012; accepted after revision 2 January 2013; online publish-ahead-of-print 22 January 2013

Aims To explore the potentiality of cardiovascular magnetic resonance (CMR) in the quantitative evaluation of mitral valve annulus (MVA) and tricuspid valve annulus (TVA) morphology and dynamics.

Methods and results CMR was performed in 13 normal subjects and 9 patients with mitral ($n = 7$) or tricuspid regurgitation ($n = 2$), acquiring cine-images in 18 radial long-axis planes passing through the middle of MVA or TVA. A novel algorithm was used to obtain dynamic three-dimensional (3D) reconstruction of MVA and TVA. Analysis was feasible in all cases, allowing accurate 3D annular reconstruction and tracking. The 3D area increased from systole [MVA, median = 10.0 cm^2 (first quartile = 8.6, third quartile = 11.4); TVA, 11.2 cm^2 (8.8–13.2)] to diastole [MVA, 10.6 cm^2 (9.4, 11.7); TVA, 11.9 cm^2 (9.2–13.5)], with TVA larger than MVA. While the longest diameter showed similar systolic and diastolic values, the shortest diameter elongated from systole [MVA, 30 mm (29–33); TVA, 33 mm (31–36)] to diastole [MVA, 31 mm (29–32); TVA, 36 mm (33–39)]. Also, TVA became more circular than MVA. TVA showed lower peak systolic excursion in the septal [15.9 mm (13.0–18.5)] and anterior regions [17.9 mm (12.2–20.7)] compared with the posterior [21.9 mm (18.6–24.0)] segment. Values in MVA were smaller than in TVA, slightly higher in anterior [11.2 mm (9.5–13.0)] than in posterior [12.4 mm (10.2–14.6)] segments. Valvular regurgitation was associated with enlarged, flattened, and more circular annuli.

Conclusion The applied method was feasible and accurate in normal and regurgitant valves, and may potentially have an impact on diagnosis, improvement of surgical techniques and design of annular prostheses.

Keywords Annular geometry • Cardiovascular magnetic resonance • Mitral valve annulus • Tricuspid valve annulus

Introduction

Atrioventricular valves are complex anatomical structures including annulus, leaflets, papillary muscles, and chordae tendinae, and alterations involving any of these components could affect valve competency. In particular, the annulus plays an important structural and functional role and it has been demonstrated that annular dilation represents the underlying mechanism of regurgitation in the majority of cases.[1–4] Therefore, the detailed knowledge of the three-dimensional (3D) morphology and dynamics of the mitral valve annulus (MVA) and tricuspid valve annulus (TVA) under pathophysiological conditions may potentially have an impact on the diagnosis, as well as on the improvement of surgical techniques and design of annular prostheses.[5] Several studies, performed using different imaging techniques both in animal and human models, have already investigated the morphology and dynamics of the MVA,[6–9] whereas the TVA has been less extensively studied.[10,11]

The aims of the present study were: (i) to demonstrate the feasibility of dynamic 3D reconstruction of MVA and TVA, based on cardiovascular magnetic resonance (CMR) imaging; (ii) to describe the 3D morphology and motion of both MVA and TVA in normal

* Corresponding author. Tel: +39 02 5800 2011; Fax: +39 02 5800 2287, Email: fmaffessanti@ccfm.it

subjects; (iii) to qualitatively compare these findings with those obtained in patients affected by mitral or tricuspid insufficiency.

Methods

A group of 22 subjects (15 males, mean age 44 ± 16 years) was prospectively enrolled among inpatients and employees at Centro Cardiologico Monzino IRCCS (Milan, Italy). Thirteen subjects were considered as a normal at CMR evaluation in the absence of regional or global left ventricular (LV) and/or right ventricular (RV) dysfunction, normal atrial dimensions, primary or secondary mitral and/or tricuspid regurgitation more than trace, and atrial tachyarrhythmia. Of the remaining subjects, seven had isolated mitral regurgitation of different degrees, whereas two had moderate or severe isolated tricuspid regurgitation. Demographic and clinical characteristics of the population are listed in *Table 1*. All subjects were in sinus rhythm.

For all subjects, exclusion criteria were standard contraindications to CMR. The protocol was approved by the Institutional Review Board, and informed consent was obtained from each participant.

CMR imaging

CMR studies were performed using a 1.5 T scanner (Discovery MR450, GE Healthcare, Milwaukee, WI, USA) equipped with an eight-element torso coil and retrospective ECG triggering for capture of the entire cardiac cycle. All CMR scans were performed by the same operator.

Steady-state free precession end-expiratory breath hold cine-images were acquired in approximated horizontal and vertical long-axis planes to reach the best orientation for obtaining a stack of short-axis slices covering the entire LV and RV cavities. The following sequence parameters were used: echo time 1.57 ms, 15 views per segment, repetition time 3.2 ms without view sharing, slice thickness 8 mm, no gap between slices, and pixel size 1.4 × 1.4 mm. Using the short-axis image in correspondence of the atrioventricular plane as a guidance, the centre of the MVA was identified and used to acquire 18 radial images (spatial resolution 0.74 mm, slice thickness 6 mm, matrix 512 × 512) evenly rotated along the long-axis ideally passing through the mid-point previously selected, as shown in *Figure 1*, top left. A similar strategy was adopted for the TVA. Each acquired

Table 1 Clinical characteristics of the study population on an individual basis

				Left ventricle			Right ventricle			
Gender	Age	BSA	HR	EDV	ESV	EF	EDV	ESV	EF	Diagnosis
M	40	2.0	70	138	57	59	153	66	57	Normal
F	26	1.6	76	104	34	67	116	41	64	Normal
F	27	1.4	96	85	29	66	103	38	63	Normal
M	24	1.7	74	159	47	71	176	72	59	Normal
M	51	1.9	60	119	60	49	155	54	65	Normal
M	29	2.1	66	145	53	63	173	84	52	Normal
M	27	1.9	48	169	71	58	201	97	52	Normal
M	26	1.5	80	121	51	57	125	63	49	Normal
M	46	2.3	62	118	40	66	125	63	49	Normal
F	34	1.7	72	134	63	53	121	63	48	Normal
M	23	1.8	74	156	64	59	148	65	56	Normal
F	59	1.5	74	127	52	59	109	47	57	Normal
M	42	1.8	75	156	49	69	157	48	69	Normal
M	74	1.6	58	129	53	59	106	43	60	Mild MVR: RegV = 10 mL/beat, RegF = 13%; organic, anterior leaflet prolapse, hypomobile posterior leaflet;
M	67	2.0	48	306	206	33	113	51	55	Moderate MVR: RegV = 40 mL/beat, RegF = 40%; idiopathic dilated cardiomyopathy
F	52	1.6	88	118	32	73	94	31	68	Mild-moderate MVR: RegV = 20 mL/beat, RegF = 24%; organic prolapse associated with thickened leaflets
M	60	2.1	62	228	150	34	168	77	54	Mild-moderate MVR; RegV = 20 mL/beat, RegF = 26%, ischaemic dilated cardiomyopathy
M	47	1.8	54	262	85	67	162	68	58	Severe MVR: RegV = 90 mL/beat, RegF = 51%; organic prolapse associated with chordal rupture
M	62	1.7	86	150	44	71	86	39	54	Severe MVR: RegV = 62 mL/beat, RegF = 58%; organic prolapse
M	60	1.9	72	347	183	47	134	41	69	Moderate-severe MVR: 67 mL/beat, RegF = 41%; idiopathic dilated cardiomyopathy
F	55	1.5	63	99	31	69	228	142	38	Mild-moderate TVR; RegV = 23 mL/beat, RegF = 27%; primary severe pulmonary hypertension
F	45	1.8	61	126	41	67	313	174	45	Moderate-severe TVR; RegV = 55 mL/beat, RegF = 40%; right ventricular dilation

BSA, body surface area; EDV, end-diastolic volume; EF, ejection fraction; ESV, end-systolic volume; F, female; M, male; MVR, mitral valve regurgitation; RegF, regurgitant fraction; RegV, regurgitant volume; TVR, tricuspid valve regurgitation.

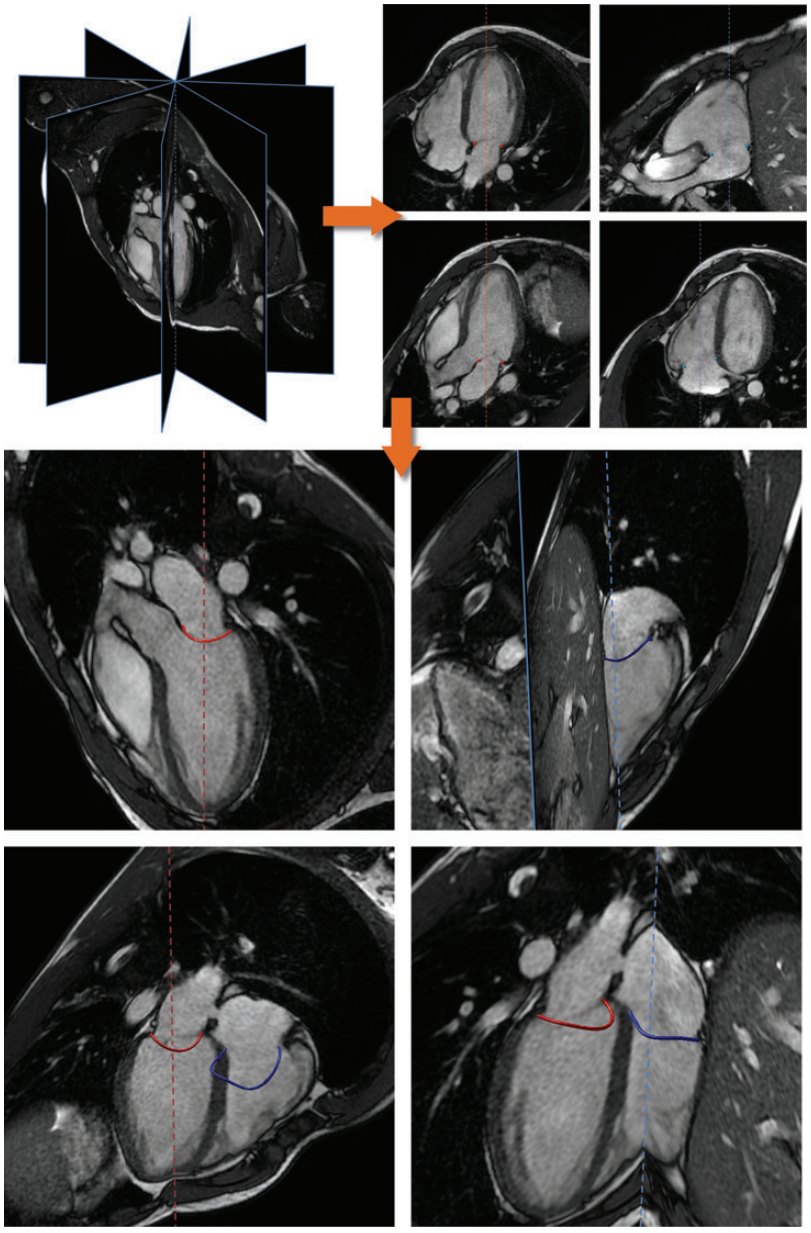

Figure 1 Schematic of image acquisition (top left panel) and post-processing: annular points were manually placed in each plane at end-diastole and end-systole (top right panels) and automatically tracked throughout the cardiac cycle. Finally, three-dimensional mitral (red) and tricuspid annuli (blue) were obtained.

plane included 20–30 phases over the cardiac cycle during repeated 10–15 s breath holds, resulting in a total of 360–540 images for each acquisition.

Finally, to calculate systemic and pulmonary flow phase-contrast velocity mapping (velocity encoding 250 cm/s) was performed through a plane transecting, respectively, the short-axis of the ascending aorta and the pulmonary artery above the valves.

LV and RV volumes were calculated with the Simpson rule by summation of manually delineated end-diastolic (ED) and end-systolic (ES) areas on each short-axis slice, including the papillary muscles, multiplied by slice thickness. Stroke volume and ejection fraction were defined as the difference between ED and ES volumes and as the stroke volume to ED volume ratio, respectively.

Systemic and pulmonary flows were quantified defining a region of interest in the phase contrast images and integrating the flow velocity over the entire cardiac cycle.

All measurements were performed using a dedicate post-processing software (AW 4.5, Report Card 4.0, GE Healthcare, Milwaukee, WI, USA).

Mitral and tricuspid regurgitant volumes were derived as the difference between LV and RV stroke volume vs. systemic and pulmonary flows. Severity of valvular regurgitation was graded in accordance with current echocardiographic recommendations.[12]

3D reconstruction of valvular annulus and measurements

Custom software, developed in the Matlab environment (Mathworks, Inc., Natick, MA, USA), was used to describe annular morphology and dynamics. Briefly, the ED and ES positions of two annular points were manually marked in correspondence of leaflet insertions in each plane (*Figure 1*, top right). Additional single points were placed in the centre of the aortic and pulmonary valves, to be used as an anatomic reference for the identification of different annular regions. Finally, the annular points were automatically tracked throughout the cardiac cycle using an algorithm based on normalized cross-correlation. Tracking was performed using square features, 10 pixels width, centred in each annular point, and normalized cross-correlation was evaluated for regions of 20 pixels width surrounding the feature in the adjacent frames; the position of the annular point was estimated as the maximum of the cross-correlation matrix. The coordinates of the obtained trajectories were transformed in the 3D space, the annulus obtained by fitting a least-squares spline and superimposed over the original data for visual verification (*Figure 1*, bottom).

Several measurements were calculated from the obtained 3D annulus (*Figure 2*):

(i) the two main diameters: anterior–posterior (AP) and anterolateral-posteromedial (AL-PM) for MVA, and AP and septal-medial (SM) (connecting the mid-point of the septal region to the opposite point on the free-wall) for TVA;

(ii) eccentricity, defined as the ratio AP/AL-PM for MVA, or SM/AP for TVA, where values close to one represent a more circular shape;

(iii) height, as the height of the bounding box containing the annulus;

(iv) the 3D area, as the area of the minimum surface spanning the annulus and passing through the annular mid-point;

(v) projected area, as the annulus area projected on the fitting x–y plane;

(vi) annular perimeter;

(vii) planarity index, defined as the ratio of height to major diameter in percentage, equal to zero for a flat MV and increasing when the MV saddle shape was more pronounced;[13]

(viii) based on annular dynamics, peak systolic excursion (PSE) was defined as the highest point reached at end-systole, considering the ED position as baseline; PSE values were obtained for each of the considered reference points along the annulus, and then averaged to obtained mean MVA and TVA values. Also, to evaluate regional differences in motility, the MVA was subdivided into AP segments, whereas TVA was subdivided into anterior, posterior and septal regions; PSE values were also computed separately in each of these sectors.

Data analysis

Data, when not on an individual basis, are expressed as median (first to third quartile). The Wilcoxon rank-sum test was applied to test differences between the systolic and diastolic values, or between MVA and TVA; the Kruskal–Wallis test was used to investigate regional differences in PSE.

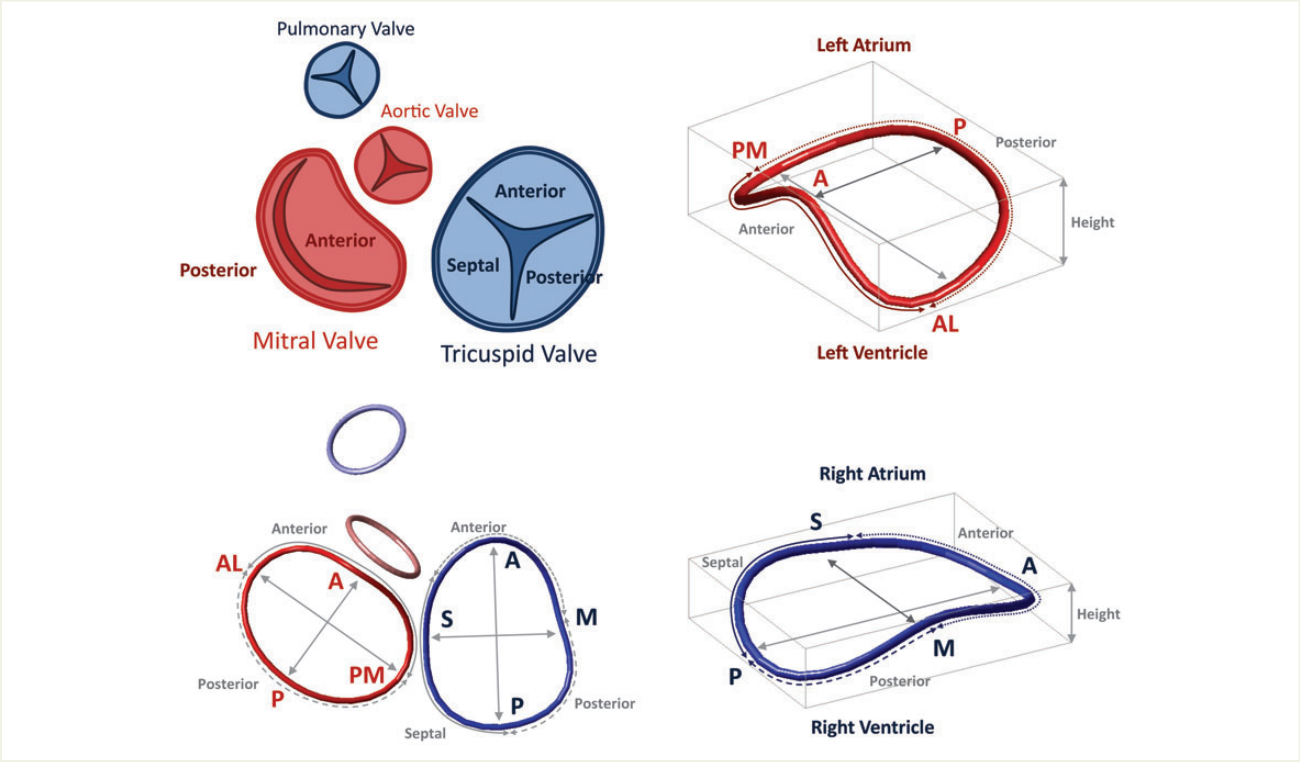

Figure 2 Left: the anatomical reciprocal position of the aortic, mitral, pulmonary and tricuspid valves as seen from the atria (top), and an example of the reconstructed models on a normal subject (bottom). Right: mitral (top) and tricuspid (bottom) annuli and the bounding box used to calculate annular diameters and height. Solid, dotted, and dashed lines represent different annular regions. AL-PM, anterolateral-posteromedial; AP, antero-posterior; SM, septal-medial.

Accuracy of the tracking algorithm was defined as the percentage of points correctly positioned by the algorithm as visually judged by an expert cardiologist in a randomly chosen subset of 10 patients (3600 images).

To assess the reproducibility of the obtained measurements, the analysis was repeated by a second-independent observer, blinded to the first observer's results, in a randomly chosen subgroup of 10 data set (five MVA, five TVA). Inter-observer variability was studied, using the Pearson r^2 coefficient of correlation, Bland–Altman analysis, and intra-class correlation coefficient. Also, the mean Euclidean distance between each pair of annuli obtained by the two observers was computed and then averaged to obtain the mean distance between the two 3D reconstructions.

Results

CMR acquisition and semiautomatic image processing took ~9 and 10 min per annulus, including initialization, tracking, and manual correction, if required. Analysis was feasible in all patients, and position of the tracked points was visually judged as correct in 3122 out of 3600 images (87% accuracy).

Annular morphology

An example of the temporal evolution of TVA and MVA in a healthy volunteer, together with the changes in 3D and projected areas, diameters, and height in the same subject, is depicted in *Figure 3*. The MVA and TVA area strictly correlated, showing a biphasic pattern, with one peak approximately located at mid-systole and the other, with higher amplitude, at late diastole. As expected, the 3D annular area was consistently higher than the projected area both for MVA and TVA. Similar patterns were observed for diameters, with AL-PM longer than AP in MVA and AP longer than SM in TVA. Whereas MVA height showed a late systolic peak, it was not possible to recognize a clear pattern in TVA, even if a slight decrease was noticeable during diastole.

Table 2 lists the minimum and maximum values for each parameter in the healthy volunteers, as well as their mean systolic and diastolic values, confirming the findings observed in *Figure 3*. In detail, 3D and projected areas of MVA and TVA significantly increased from systolic to diastolic values; this enlargement was associated with an elongation of the TVA, but not MVA, perimeter. TVA values of area and perimeter were greater than in MVA. The two annular diameters showed different behaviours: while the longest diameter (AL-PM for MVA, AP for TVA) did not change significantly from systole to diastole, the shortest diameter (AP for MVA, SM for TVA) elongated in diastole, significantly for TVA. Also, the SM diameter for TVA was greater than its mitral counterpart, AP, whereas the longest diameters were similar. Eccentricity of both annuli was found higher during diastole than in systole, with TVA significantly more circular than MVA. MVA was showed an increased height than TVA, both during systole and diastole. The differences in height and diameters implied a more planar shape of both annuli in diastole than in systole, with MVA more saddle shaped than TVA.

Annular dynamics

In *Figure 3A*, the annuli are depicted in their ED configuration, together with the trajectories of the tracked points, each colour coded by the corresponding PSE. It is possible to notice different regional motion in the two annuli, with 'cold' and almost uniform motion for the MVA, whereas TVA presents values similar to the mitral ones in the septal region only, and a larger dynamics in the AP segments, corresponding to the RV free wall. Also, it is possible to observe a bulge on the trajectory in correspondence of atrial contraction, giving evidence of the sphincteric function of both the annuli.

Figure 4, top panels, depicts the mean annular displacement of TVA and MVA throughout the cardiac cycle computed from all the normal subjects. Both curves have a similar pattern, with an ES peak, followed by a diastolic decrease, and a plateau phase, interrupted by an abrupt slope in concomitance of the *P*-wave.

When considering the regional PSE (*Figure 4*, bottom), TVA showed lower PSE values in the septal [15.9 mm (13.0, 18.5)] and anterior [17.9 mm (12.2, 20.7)] regions compared with the posterior segment 21.9 mm (18.6, 24.0)], which in turns showed the highest displacement. Conversely, MVA showed smaller PSE, without a slight difference between the anterior [11.2 mm (9.5, 13.0)] and posterior [12.4 mm (10.2, 14.6)] regions.

Annular morphology in presence of regurgitation

The analysis was feasible also in all the patients with different degrees of mitral or tricuspid regurgitation and the results are summarized in *Table 3*. A qualitative comparison with the values relevant to normal subjects (*Table 2*) shows that, in patients with mitral regurgitation, MVA was enlarged in terms of area, both 3D and projected, perimeter and AP-LM diameters. These abnormalities were associated with increased eccentricity and flattened height, while TVA morphology was apparently not affected by mitral insufficiency. Also, in the presence of mitral regurgitation, MVA PSE values [9.3 mm (7.0, 13.7); anterior: 8.4 mm (6.2, 12.6); posterior: 10.0 mm (7.9, 14.5)] were smaller than those measured in normal subjects, and this was associated with slightly reduced TVA PSE values [mean: 14.9 mm (9.3, 21.3); septal: 10.8 mm (7.0, 15.9); posterior: 16.6 mm (11.8, 20.3); anterior: 17.1 mm (10.3, 25.5)].

Specular observations can be made in the presence of severe tricuspid regurgitation: TVA was strongly enlarged in terms of area, perimeter and diameters, with reduced height despite a planarity index similar to controls, MVA values were in the normal range. Also, TVA displacement (mean: 12.5 mm; septal: 11.7 mm; posterior: 12.7 mm; anterior: 12.8 mm), but not MVA (mean: 13.8 mm; posterior: 14.7 mm; anterior: 12.7 mm), was found reduced in the presence of severe tricuspid insufficiency. The values obtained in the subject with mild-moderate tricuspid regurgitation were similar to those found in normal subjects.

Reproducibility

The mean Euclidean distance between the repeated 3D reconstructions was 1.3 mm (95% confidence interval: 0.3–3.2 mm). Inter-observer reproducibility analysis demonstrated good to excellent concordance (*Table 4*), without significant bias and narrow limits of agreement. In detail, reproducibility was optimal for displacement, area, perimeter, and the longest diameter (ICC >0.97), whereas the other parameters, despite good correlations, were slightly less reproducible.

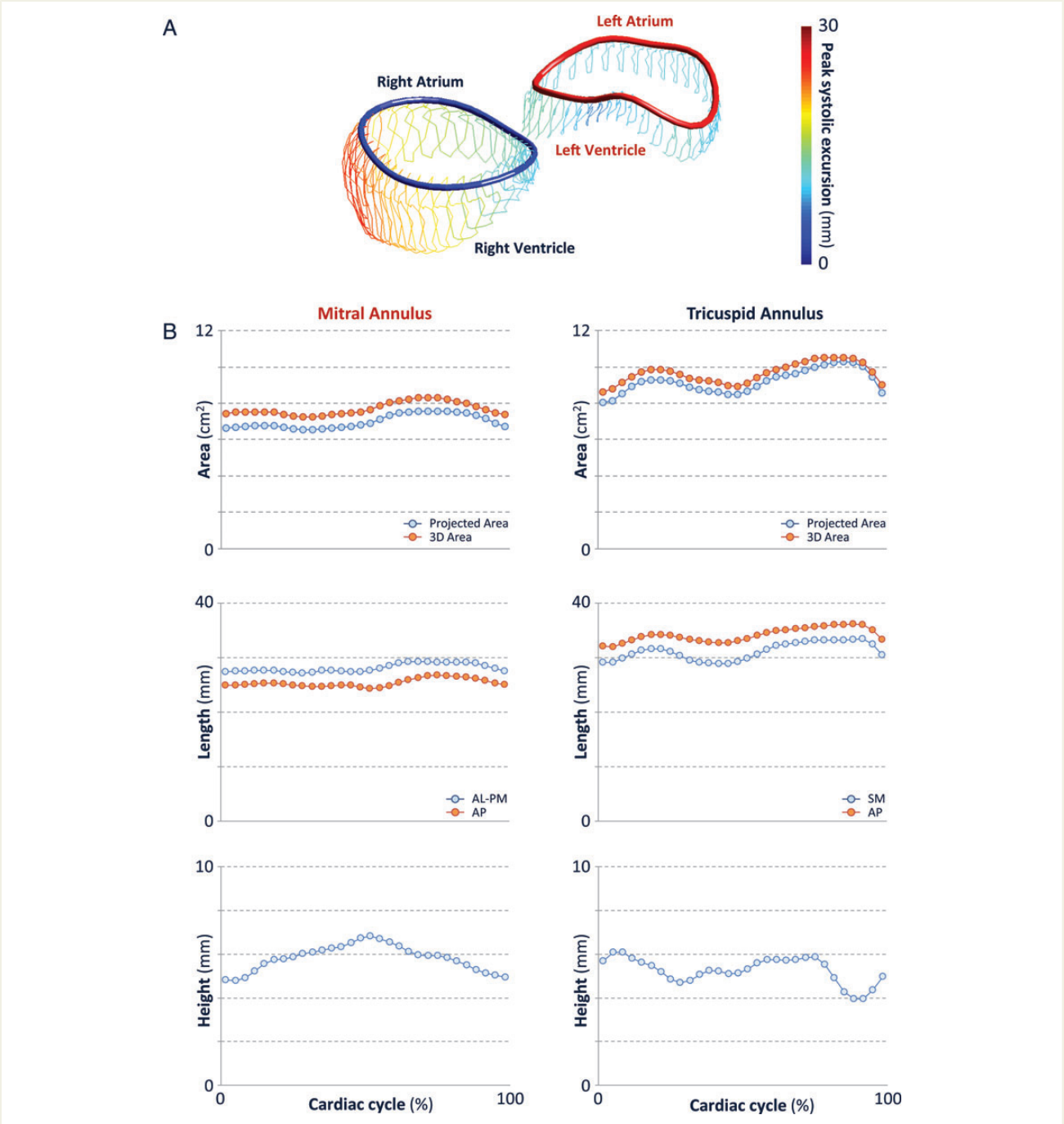

Figure 3 (*A*) Example of the temporal evolution of mitral (red) and tricuspid (blue) annulus position in the cardiac cycle; (*B*) Changes in annular 3D and projected areas, diameters, and height during the cardiac cycle. AL-PM, anterolateral-posteromedial; AP, antero-posterior; SM, septal-medial.

Discussion

The present study aimed at obtaining a morphological and functional description of MVA and TVA, while evaluating the feasibility and reproducibility of a novel semi-automatic algorithm based on cine CMR images for point tracking and 3D reconstruction. The methodology was feasible in all cases, accurate when compared with manual analysis performed by an expert cardiologist, and highly reproducible. To the best of our knowledge, this study constitutes the first attempt to quantify in the same subject both MVA and TVA morphology and motion using CMR and a semi-automatic approach.

The interest towards the morphological and functional assessment of the atrioventricular valves is not purely speculative but driven by clinical implications. Indeed, valvular regurgitation is

Table 2 Morphologic measurements obtained for mitral and tricuspid annuli in normal subjects

	Mitral annulus	Tricuspid annulus	*P*-value
Three-dimensional area (cm^2)			
Minimum	9.1 (8.2–10.1)	10.3 (8.4–11.0)	0.18
Maximum	10.8 (9.6–12.6)	13.0 (10.4–15.0)	<0.01
Systolic	10.0 (8.6–11.4)	11.2 (8.8–13.2)	<0.01
Diastolic	10.6 (9.4–11.7)*	11.9 (9.2–13.5)*	<0.01
Projected area (cm^2)			
Minimum	8.9. (7.9–9.8)	10.0 (7.9–10.6)	0.07
Maximum	10.4 (9.2–12.1)	12.7 (10.3–14.1)	<0.01
Systolic	9.2 (8.0–10.6)	10.6 (7.9–12.0)	<0.01
Diastolic	9.7 (8.9–11.2)*	11.3 (8.6–12.7)*	<0.01
Perimeter (mm)			
Minimum	112 (104–119)	114 (105–124)	0.22
Maximum	121 (113–131)	128 (116–142)	<0.01
Systolic	115 (106–123)	119 (107–128)	<0.01
Diastolic	116 (111–125)	123 (111–131)*	<0.01
Shortest diameter (mm)			
Minimum	28 (26–30)	32 (29–34)	0.04
Maximum	33 (31–35)	38 (35–40)	<0.10
Systolic	30 (29–33)	33 (31–36)	<0.01
Diastolic	31 (29–32)	36 (33–39)*	<0.01
Longest diameter (mm)			
Minimum	35 (33–40)	33 (31–33)	0.08
Maximum	39 (36–43)	42 (36–47)	0.09
Systolic	37 (34–40)	37 (33–41)	0.65
Diastolic	38 (35–41)	39 (33–43)	0.94
Eccentricity			
Minimum	0.73 (0.71–0.81)	0.85 (0.81–0.91)	0.05
Maximum	0.92 (0.85–0.94)	0.97 (0.88–1.00)	0.02
Systolic	0.82 (0.76–0.89)	0.91 (0.81–0.97)	<0.01
Diastolic	0.85 (0.78–0.89)*	0.93 (0.87–0.99)*	<0.01
Height (mm)			
Minimum	4.7 (3.6–6.6)	3.7 (2.4–3.8)	0.06
Maximum	9.3 (7.8–10.2)	7.2 (6.3–9.2)	0.13
Systolic	7.7 (6.8–9.2)	5.6 (4.4–7.1)	<0.01
Diastolic	6.9 (4.9–8.3)*	5.0 (4.0–6.0)*	0.01
Planarity index (%)			
Minimum	13 (9–19)	9 (6–10)	0.12
Maximum	25 (22–28)	20 (17–25)	0.11
Systolic	21 (17–25)	16 (11–20)	<0.01
Diastolic	17 (14–23)*	12 (11–14)*	0.01

Values expressed as median (first quartile, third quartile).
P-value refers to mitral VS tricuspid measurements, the Wilcoxon Signed-rank test for non-independent samples.
*$P < 0.05$, systolic vs. diastolic values, the Mann–Whitney *U* test for independent samples.

frequently due not to a primary disease, but rather to an insufficient leaflets coaptation associated with dilation and geometric distortion of the annulus.[3] Also, geometric parameters, such annular diameter and height, have been identified as determinants of residual regurgitation or recurrence of valve incompetency after surgical repair.[2,14,15] Thus, a deep and complete understanding of annular morphology and motion could have potential effects on pathophysiological knowledge, and in turn on diagnosis and surgical treatment.[5]

Several studies have already addressed the morphological evaluation of the atrioventricular valves, from pioneer works using 2D echocardiography,[6,16] to more recent approaches using computed tomography or real-time 3D echocardiography.[9,17,18] The latter allowed the characterization of 3D annular anatomy without the need of cumbersome reconstruction from multiple 2D images, avoiding the potential inaccuracies arising from an imprecise localization of the probe. Despite these advantages, the feasibility of TVA assessment by real-time 3D echocardiography has been shown suboptimal, with an adequate 3D visualization in 90% of normal subjects with good 2D images.[18] CMR imaging is a non-invasive technique that can provide a concrete opportunity for the *in vivo* detailed characterization of valvular structures,[19–21] with a proven accuracy compared with transoesophageal echocardiography as a reference technique.[22] The main limitation of CMR is represented by its intrinsic 2D nature that can prevent the assessment of valvular structures in their 3D complexity. However, the capability of imaging and precisely localizing an unlimited number of planes, allowed to reconstruct a 3D model of the MVA by the acquisition of multiple rotated long-axis cine images.[23,24] Using a similar acquisition method, the present study introduces two important novelties compared with our previous works[23,24] (i) the combined morphological analysis of MVA and TVA, the latter not investigated previously, acquired during the same CMR examination; (ii) current analysis considers not only the ED and ES annular configuration, but their dynamic behaviour allowing a more temporally refined characterization of annular morphology and trajectory during the cardiac cycle, requiring the same user interaction.

Results demonstrated that MVA and TVA are highly dynamic structures, with similar behaviours but also with some peculiarities. In detail, area revealed a biphasic pattern, with a first peak at end-systole, which we may hypothesize related to atrial filling, and then a second and higher peak in late diastole, in conjunction with active atrial contraction. These changes, in agreement with those reported in previous studies conducted both in animal models and in humans,[25–28] evidence the double role of the atrioventricular annuli: structural, when the valve is closed and its area follows the atrial volume, and functional, when the valve acts like a sphincter adapting to the atrial flow. Consistently with literature, changes in annular dimension are not uniform but they happen according to a preferred direction.[3] Indeed, results show that diastolic annular enlargement happens almost exclusively in the AP direction for the MVA and in the SM for the TVA, while similar changes were not observed in the longest diameter direction (*Table 2*). This asymmetrical enlargement is likely to be related to the greater distensibility of the RV free-wall and the posterior wall of the left ventricle, compared with the stiffness of the septal region, mainly fibrous and structural. In addition, we demonstrated that annular height significantly decreases during diastole, and this annular flattening is confirmed by the planarity index. Similarly, when annular dilation is not physiological but associated with the loss of valve competency, MVA and TVA dilate along their shortest diameter

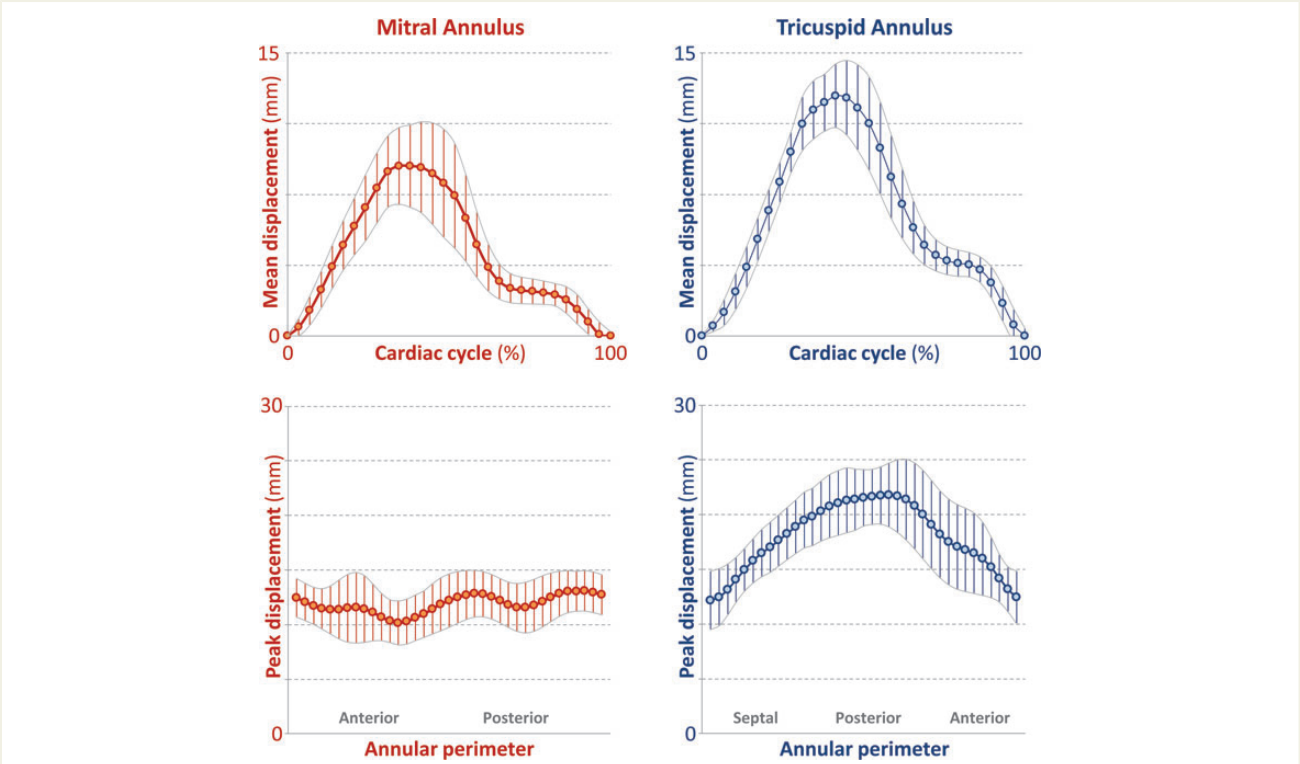

Figure 4 The mean annular displacement of tricuspid and mitral annulus throughout the cardiac cycle (top), and peak displacement as a function of the annular region on the perimeter (bottom). Whiskers represent standard deviation.

as observed in our patients, in agreement with results obtained on larger populations.[3,4,13] Summarizing, both MVA and TVA undergo similar morphological changes, increasing their area during diastole and reaching the peak in correspondence of atrial contraction. Annular enlargement happens preferentially along the shortest diameter direction, increasing eccentricity (i.e. the annuli become more circular), and this is associated with annular flattening.

Despite the evidenced similarities, MVA and TVA have some different aspects. The TVA area was larger than MVA, as a consequence of a greater short diameter in the presence of comparable long diameters. Also, TVA is more circular and flat than MVA, and we may hypothesize that these differences are related to the different pressure between the left and the right side: a greater area allows an adequate diastolic filling flow even in the presence of a low transvalvular pressure gradient. The use of a 3D approach and adequate temporal resolution allowed us to evidence dissimilarities in annular motion. First, the two mean displacement curves (*Figure 4*, top) have similar envelope, but different amplitudes. Moreover, MVA motion was almost uniform along the perimeter, with values similar to those reported in larger series using M-mode echocardiography (11.4 ± 3.1 mm).[29] Conversely, TVA showed a more complex dynamics, minimal in the antero-septal region and maximal in the posterior region, with values similar to those reported for TAPSE in normal subjects.[30] We can assume that the fibrous skeleton connecting the MVA and TVA increases the stiffness and thus reduces annular motility, resulting in the same PSE values for TVA in the AP region and MVA in the anterior segment (*Figure 4*, bottom). Conversely, the lack of such constraint in correspondence of the RV free-wall allows larger motion of the AP TVA. TVA motion could thus be described as a combination of a translational component, represented by the valvular plane displacement, and a rotational component, equal to zero where the TVA connects to the fibrous tissue, and maximum in correspondence of the RV free-wall. In conjunction with the distinct anatomic structures of the two annuli, the pattern of contraction of the two ventricles, predominantly twisting for the left and longitudinal for the right ventricle, may influence and contribute to explain the observed differences in annular motion.

The feasibility of this approach was also tested in patients with valvular regurgitation and, as expected, the presence of valve insufficiency was associated with enlarged, flattened, and more circular annuli.

Clinical implications

CMR is the reference technique for ventricular volumes and function assessment, detailed evaluation of biventricular pathologies, and a complementary method in valve disease, with proven value in regurgitant volume quantification. The demonstrated feasibility of 3D dynamic evaluation of MVA and TVA could constitute an additional tool for a comprehensive morphofunctional assessment of cardiac chambers and valves in specific pathologies. Moreover, as innovative surgical and interventional procedures require an accurate description of these structures, the described

Table 3 Morphologic measurements obtained for mitral and tricuspid annuli in patients with different degrees of mitral valve (MVR) or tricuspid valve regurgitation (TVR)

	MVR ($n = 7$)		TVR ($n = 2$)	
	Systole	Diastole	Systole	Diastole
Mitral valve annulus				
3D area (cm^2)	12.2 (8.9–19.0)	13.0 (9.3–19.8)	7.6; 8.8	8.2; 9.1
Projected area (cm^2)	11.9 (8.5–17.6)	12.6 (9.0–18.7)	7.3; 8.5	7.9; 9.0
Perimeter (mm)	127 (110–160)	129 (110–163)	99; 107	105; 109
AP diameter (mm)	35 (28–42)	37 (31, 43)	27; 31	27; 32
AL-PM diameter (mm)	40 (32–50)	41 (33–51)	33; 34	35; 35
Height (mm)	5.5 (3.2–9.1)	4.0 (1.3–7.2)	5.2; 2.7	3.6; 2.0
Eccentricity	0.88 (0.76–0.99)	0.89 (0.76–0.99)	0.84; 0.91	0.79; 0.91
Planarity index (%)	14 (8–18)	10 (4–14)	16; 8	10; 6
Tricuspid valve annulus				
3D area (cm^2)	10.0 (8.8–14.0)	10.5 (9.1–14.3)	10.7; 19.4	11.0; 19.9
Projected area (cm^2)	10.6 (8.4–13.6)	11.2 (8.9–14.2)	10.4; 19.0	10.8; 19.6
Perimeter (mm)	121 (110–140)	124 (113–142)	117; 159	119; 161
SM diameter (mm)	32 (31–34)	32 (26–35)	36; 50	36; 52
AP diameter (mm)	40 (35–48)	42 (36–49)	37; 48	38; 48
Height (mm)	5.8 (5.2–6.8)	5.3 (3.5–6.2)	5.7; 6.3	5.3; 6.1
Eccentricity	0.84 (0.70–0.94)	0.87 (0.75–0.95)	0.97; 0.92	0.97; 0.96
Planarity index (%)	16 (11–20)	13 (8–16)	16; 13	14; 13

Values expressed as median (minimum, maximum) for the TVR group, and on individual basis for the patients with MVR (mild-moderate TVR; moderate-severe TVR).
3D, three-dimensional; AL-PM, anterolateral-posteromedial; AP, anterior-posterior; SM, septal-medial.

Table 4 Results of inter-observer reproducibility analysis, in terms of Pearson's correlation coefficient R^2, bias in Bland–Altman analysis and intra-class correlation coefficient (ICC)

	r^2	Bias	ICC
Displacement (mm)	0.997	0.05 (−0.61, 0.72)	0.998 (0.998 –0.999)
Area (cm^2)	0.988	−0.37 (−0.98, 0.23)	0.973 (0.661 –0.992)
Perimeter (mm)	0.988	−2.7 (−6.8, 1.5)	0.973 (0.627 –0.992)
Shortest diameter (mm)	0.913	−0.7 (−2.4, 1.1)	0.927 (0.747 –0.968)
Longest diameter (mm)	0.988	0.3 (−1.1, 1.7)	0.989 (0.981 –0.993)
Eccentricity	0.930	−0.02 (−0.08, 0.04)	0.930 (0.811 –0.966)
Height (mm)	0.879	−0.5 (−3.0, 2.0)	0.923 (0.869 –0.952)

95% confidence interval is reported in brackets.

approach could have an impact on the diagnosis, on the improvement of surgical techniques, as well as on the design of annular prostheses.

Limitations

This is an observational study in which we applied 3D analysis of MVA and TVA in a relatively small group of healthy volunteers and patients with different degrees of valvular regurgitation. The limited population size and the different degree of LV and RV tricuspid dysfunction did not allow to investigate the relevance of ventricular function on annular motion. A larger study is needed to go beyond feasibility, by proving the clinical potentials of the proposed approach in selected populations, analysing the association between clinical and demographic parameters with the obtained annular parameters. Also, we were not able to compare CMR measures with similar echocardiographic parameters, in particular tricuspid annulus PSE.

Different regions for TVA and MVA were identified on the basis of the anatomical reference and not on leaflet commissures.

Conclusion

To the best of our knowledge this is the first study comparing MVA and TVA morphology and dynamics in the same subject and with imaging performed in the same conditions. The use of CMR, despite a prolonged but still acceptable acquisition and processing time, allowed imaging every plane with high spatial resolution, and also could provide values for ventricular function and flow. The applied method revealed feasible in both normal subjects and patients with mitral or tricuspid regurgitation, accurate as judged by an expert cardiologist and highly reproducible.

Conflict of interest: Dr Gianluca Pontone received speaker fees and reimbursement for travel expenses from GE Healthcare. Dr Daniele Andreini received speaker fees and reimbursement for travel expenses from GE Healthcare.

All other authors reported that they have no relationships relevant to the contents of this paper to disclose.

References

1. Kaul S, Pearlmann J, Touchstone DA, Esquival L. Prevalence and mechanisms of mitral regurgitation in the absence of intrinsic abnormalities of the mitral leaflets. *Am Heart J* 1989;**118**:963–72.
2. Sagie A, Schwammenthal E, Padial LR, Vazquez de Prada JA, Weyman AE, Levine RA. Determinants of functional tricuspid regurgitation in incomplete tricuspid valve closure: Doppler color flow study of 109 Patients. *J Am Coll Cardiol* 1994;**24**:446–53.
3. Dreyfus GD, Corbi PJ, Chan KM, Bahrami T. Secondary tricuspid regurgitation or dilatation: which should be the criteria for surgical repair? *Ann Thorac Surg* 2005; **79**:127–32.
4. Ton-Nu TT, Levine RA, Handschumacher MD, Dorer DJ, Yosefy C, Fan D *et al.* Geometric determinants of functional tricuspid regurgitation: insights from 3-dimensional echocardiography. *Circulation* 2006;**114**:143–9.
5. Badano LP, Agricola E, Perez de Isla L, Gianfagna P, Zamorano JL. Evaluation of the tricuspid valve morphology and function by transthoracic real-time three-dimensional echocardiography. *Eur J Echocardiogr* 2009;**10**:477–84.
6. Ormiston JA, Shah PM, Tei C, Wong M. Size and motion of the mitral valve annulus in man. I. A two-dimensional echocardiographic method and findings in normal subjects. *Circulation* 1981;**64**:113–20.
7. Levine RA, Handschumacher MD, Sanfilippo AJ, Hagege AA, Harrigan F, Marshall JE *et al.* Three-dimensional echocardiographic reconstruction of the mitral valve, with implications for the diagnosis of mitral valve prolapse. *Circulation* 1989;**80**:589–98.
8. Timek TA, Glasson JR, Lai DT, Liang D, Daughters GT, Ingels NB Jr *et al.* Annular height-to-commissural width ratio of annuloplasty rings *in vivo*. *Circulation* 2005; **112**(Suppl. 9):I423–8.
9. Caiani EG, Fusini L, Veronesi F, Tamborini G, Maffessanti F, Gripari P *et al.* Quantification of mitral annulus dynamic morphology in patients with mitral valve prolapse undergoing repair and annuloplasty during a 6-month follow-up. *Eur J Echocardiogr* 2011;**12**:375–83.
10. Lang RM, Mor-Avi V, Sugeng L, Nieman PS, Sahn DJ. Three-dimensional echocardiography: the benefits of the additional dimension. *J Am Coll Cardiol* 2006;**48**: 2053–69.
11. Kwan J, Kim GC, Jeon MJ, Kim DH, Thomas JD, Park KS *et al.* 3D geometry of a normal tricuspid annulus during systole: a comparison study with the mitral annulus using real-time 3D echocardiography. *Eur J Echocardiogr* 2007;**8**:375–83.
12. Zoghbi WA, Enriquez-Sarano M, Foster E, Grayburn PA, Kraft CD, Levine RA *et al.* Recommendations for evaluation of the severity of native valvular regurgitation with two-dimensional and Doppler echocardiography. *J Am Soc Echocardiogr* 2003;**16**:777–802.
13. Maffessanti F, Marsan NA, Tamborini G, Sugeng L, Caiani EG, Gripari P *et al.* Quantitative analysis of mitral valve apparatus in mitral valve prolapse before and after annuloplasty: a three-dimensional intraoperative transesophageal study. *J Am Soc Echocardiogr* 2011;**24**:405–13.
14. Min SY, Song JM, Kim JH, Jang MK, Kim YJ, Song H *et al.* Geometric changes after tricuspid annuloplasty and predictors of residual tricuspid regurgitation: a real-time three-dimensional echocardiography study. *Eur Heart J* 2010;**31**: 2871–80.
15. Park YH, Song JM, Lee EY, Kim YJ, Kang DH, Song JK. Geometric and hemodynamic determinants of functional tricuspid regurgitation: a real-time three-dimensional echocardiography study. *Int J Cardiol* 2008;**124**:160–5.
16. Tei C, Pilgrim JP, Shah PM, Ormiston JA, Wong M. The tricuspid valve annulus: study of size and motion in normal subjects and in patients with tricuspid regurgitation. *Circulation* 1982;**66**:665–71.
17. Ionasec RI, Voigt I, Georgescu B, Wang Y, Houle H, Vega-Higuera F *et al.* Patient-specific modeling and quantification of the aortic and mitral valves from 4-D cardiac CT and TEE. *IEEE Trans Med Imaging* 2010;**29**:1636–51.
18. Anwar AM, Geleijnse ML, Soliman OI, McGhie JS, Frowijn R, Nemes A *et al.* Assessment of normal tricuspid valve anatomy in adults by real-time three-dimensional echocardiography. *Int J Cardiovasc Imaging* 2007;**23**:717–24.
19. Maron MS, Olivotto I, Harrigan C, Appelbaum E, Gibson CM, Lesser JR *et al.* Mitral valve abnormalities identified by cardiovascular magnetic resonance represent a primary phenotypic expression of hypertrophic cardiomyopathy. *Circulation* 2011;**124**:40–7.
20. Stork A, Franzen O, Ruschewski H, Detter C, Müllerleile K, Bansmann PM *et al.* Assessment of functional anatomy of the mitral valve in patients with mitral regurgitation with cine magnetic resonance imaging: comparison with transesophageal echocardiography and surgical results. *Eur Radiol* 2007;**17**:3189–98.
21. Gabriel RS, Kerr AJ, Raffel OC, Stewart RA, Cowan BR, Occleshaw CJ. Mapping of mitral regurgitant defects by cardiovascular magnetic resonance in moderate or severe mitral regurgitation secondary to mitral valve prolapse. *J Cardiovasc Magn Reson* 2008;**10**:16.
22. Han Y, Peters DC, Salton CJ, Bzymek D, Nezafat R, Goddu B *et al.* Cardiovascular magnetic resonance characterization of mitral valve prolapse. *J Am Coll Cardiol Img* 2008;**1**:294–303.
23. Stevanella M, Maffessanti F, Conti CA, Votta E, Arnoldi A, Lombardi M *et al.* Mitral valve patient-specific finite element modeling from cardiac MRI: application to an annuloplasty procedure. *Cardiovasc Eng Technol* 2011;**2**:66–76.
24. Maffessanti F, Stevanella M, Votta E, Lombardi M, Parodi O, De Marchi D *et al.* Feasibility of a novel approach for 3D mitral valve quantification from magnetic resonance images. *Comput Cardiol* 2010;**37**:157–60.
25. Fukuda S, Saracino G, Matsumura Y, Daimon M, Tran H, Greenberg NL *et al.* Three-dimensional geometry of the tricuspid annulus in healthy subjects and in patients with functional tricuspid regurgitation. *Circulation* 2006;**114**(Suppl. 1): I492–8.
26. Grewal J, Suri R, Mankad S, Tanaka A, Mahoney DW, Schaff HV *et al.* Mitral annular dynamics in myxomatous valve disease. *Circulation* 2010;**121**:1423–31.
27. Fawzy H, Fukamachi K, Mazer CD, Harrington A, Latter D, Bonneau D *et al.* Complete mapping of the tricuspid valve apparatus using three-dimensional sonomicrometry. *J Thorac Cardiovasc Surg* 2011;**141**:1037–43.
28. Ring L, Rana BS, Kydd A, Boyd J, Parker K, Rusk RA. Dynamics of the tricuspid valve annulus in normal and dilated right hearts: a three-dimensional transoesophageal echocardiography study. *Eur Heart J Cardiovasc Imaging* 2012;**13**:756–62.
29. Matos J, Kronzon I, Panagopoulos G, Perk G. Mitral annular plane systolic excursion as a surrogate for left ventricular ejection fraction. *J Am Soc Echocardiogr* 2012;**25**:969–74.
30. Tamborini G, Marsan NA, Gripari P, Maffessanti F, Brusoni D, Muratori M *et al.* Reference values for right ventricular volumes and ejection fraction with real-time three-dimensional echocardiography: evaluation in a large series of normal subjects. *J Am Soc Echocardiogr* 2010;**23**:109–15.